SCIENTIFIC REPORTS

OPEN

Tuning coercive force by adjusting electric potential in solution processed Co/Pt(111) and the mechanism involved

Cheng-Hsun-Tony Chang[1], Wei-Hsu Kuo[1], Yu-Chieh Chang[1], Jyh-Shen Tsay[1] & Shueh-Lin Yau[2]

A combination of a solution process and the control of the electric potential for magnetism represents a new approach to operating spintronic devices with a highly controlled efficiency and lower power consumption with reduced production cost. As a paradigmatic example, we investigated Co/Pt(111) in the Bloch-wall regime. The depression in coercive force was detected by applying a negative electric potential in an electrolytic solution. The reversible control of coercive force by varying the electric potential within few hundred millivolts is demonstrated. By changing the electric potential in ferromagnetic layers with smaller thicknesses, the efficiency for controlling the tunable coercive force becomes higher. Assuming that the pinning domains are independent of the applied electric potential, an electric potential tuning-magnetic anisotropy energy model was derived and provided insights into our knowledge of the relation between the electric potential tuning coercive force and the thickness of the ferromagnetic layer. Based on the fact that the coercive force can be tuned by changing the electric potential using a solution process, we developed a novel concept of electric-potential-tuned magnetic recording, resulting in a stable recording media with a high degree of writing ability.

During the past decade, data storage has become one of the most pressing issues that has confronted our society and the information age. The increasing use of the cloud for the storage of digital information involves the use of hard disk drives which use magnetism for the storage and retrieval of digital information[1]. In 2014, about 0.56 billion hard disk drives that provided more than 540 exabytes of storage capacity were produced[1,2]. However, due to problems associated with increasing the storage capacity of hard disk drives, the data storage community faces the necessity of exploring and developing new concepts in attempts to increase areal density[1–3]. In recent years, extensive efforts have been devoted to exploring alternate approaches for improving the storage density of magnetic recording devices, and include two-dimensional magnetic recording (TDMR)[4,5], heat-assisted magnetic recording (HAMR)[6–9], microwave-assisted magnetic recording (MAMR)[10,11], bit-patterned magnetic recording (BPMR)[12–15], and optical switching of magnetic domains[16–18]. For instance, a broadband near-field thermal extraction device based on hyperbolic metamaterials can significantly enhance near-field energy transfer by extracting evanescent waves with arbitrarily large lateral wave vectors[6]. Near-field thermal extraction has important practical implications in HAMR[6,8]. Free-floating magnetic structures composed of *in situ* cross-linked magnetically assembled nanoparticles have been reported to retain their patterned shape during manipulation with external magnetic fields[12] while a magnetic pattern can serve as an elementary base in magnetic recording media such as BPMR[12,14]. By exploiting the field-confining capability as plasmonic nanoantennas, ferrimagnetic TbFeCo thin films have the potential for use in the optical switching of magnetic domains, while the importance of a chemically homogeneous sample structure is highlighted for optical switching-based recording technologies[16]. The diazotization of $Ru(bpy)_2(phen-NH_2)^{2+}$ in the presence of carbon nanotubes (CNT) results in the formation of nanodots on CNTs, which are capable of transducing photo stimuli into electricity and magnetism at ambient conditions, and the resultant photomagnetic CNTs are a multifunctional material that have the potential for use in in optical switching-based recording technologies[17].

[1]Department of Physics, National Taiwan Normal University, Taipei 116, Taiwan. [2]Department of Chemistry, National Central University, Jhongli 320, Taiwan. Correspondence and requests for materials should be addressed to J.-S.T. (email: jstsay@phy.ntnu.edu.tw) or S.-L.Y. (email: yau6017@ncu.edu.tw)
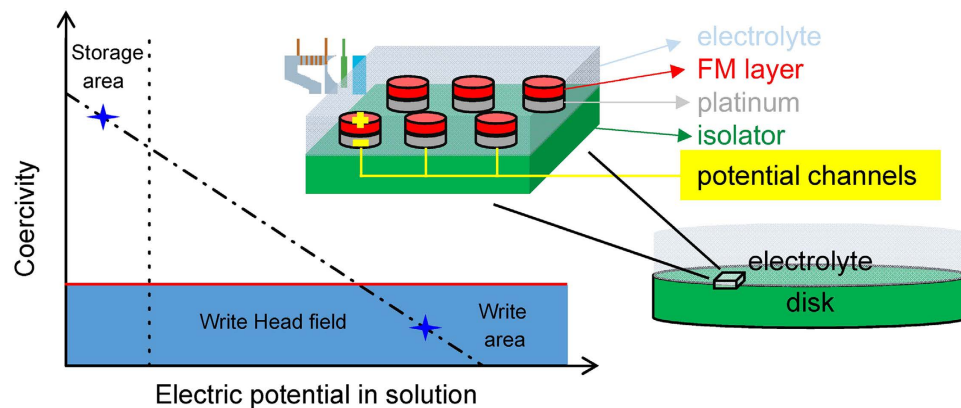
Figure 1. A schematic plot showing the storage and writing processes of EPTMR. The inset shows the designs of a magnetic recording disc for EPTMR.

Because of the higher storage density[19–21] and lower power consumption[22–25], the electric potential controlled magnetic device has attracted interest in the area of magnetic recording research. Exploring electric potential tuned magnetic devices in electrolytic conditions has also attracted great interest[24–28] because the solution process is a low cost, rapid method that is amenable for use in commercial production. In the first report of electric potential induced magnetism using FePt and FePd films in NaOH as an electrolyte, the coercive force (H_C) could be enhanced by about 4.5% by varying the electric potential between -1000 and $-400\,mV$[26]. This pioneering work has motivated researchers to further examine electric potential tuned magnetism in electrolytes[24,25,27,28]. For example, MgO(2.0 nm)/Co (0.4 nm)/Pt (1.2 nm)/Ta (3.0 nm) films show magnetic switching near the coercive field when the electric potential is tuned from $+2000$ to $-2000\,mV$ in an ionic liquid electrolyte[24]. The ferromagnetic proximity effect shows that an electric field can be used to control the magnetic moments in films made of Pd, originally a nonmagnetic element[25]. An electrochemical etching process can be used to reduce the thickness of Co films with less surface defects while the electric field induced depression of the H_C was observed to be reproducible for the case of an electrochemically etched specimen[28]. The focus of this research was on electric potential tuned magnetic phenomena that occur via the solution process with the characteristics of highly efficient controlling and ease of production.

Exploring the possible mechanisms responsible for developing electric potential tuned magnetic phenomena is an important issue in terms of developing more efficient magnetic recording devices. From the literature, the mechanisms of the electric potential tuned magnetic phenomena are mainly related to the Curie temperature[24,27,29] and magnetic anisotropy energy (MAE)[30–33]. For example, the Curie temperature of $Ga_{0.93}Mn_{0.07}As$ increases as the gate voltage sweeps from positive to negative values[29]. Based on first principle calculations of the electric field effects on magnetic anisotropy for ferromagnetic thin films on Pt(111), the MAE increases with increasing electric field and decreases with decreasing electric field[30]. Giant electric-field-assisted modifications of the interfacial magnetic anisotropy have been reported for the case of a half-metallic Heusler compound/MgO interface[31]. However, the mechanism responsible for how different thicknesses of the ferromagnetic layer (t_{FM}) affect electric potential tuned magnetic phenomena is still unclear.

In this letter, tuning the magnetic properties by an electric potential for Co/Pt(111) of nanometer thickness in the Bloch-wall regime was investigated for a solution process. For Co/Pt(111) in the Bloch-wall regime, the depression of the H_C is detected by applying a negative electric potential in an electrolytic condition. The electric potential tuned H_C and t_{FM} shows an inverse square relation that can be successfully explained using an electric potential tuning-magnetic anisotropy energy (EPT-MAE) model. For a smaller t_{FM}, the electric potential induced change of the H_C is larger, while the electric potential induced change of the MAE is again magnified. A higher controlling efficiency of the tunable H_C in thinner ferromagnetic layers was demonstrated using our apparatus. Based on the characteristics of a tunable H_C produced by changing the electric potential using a solution process, we propose a novel technique for achieving electric-potential-tuned magnetic recording (EPTMR). A schematic plot of the EPTMR with storage and writing processes is shown in Fig. 1. For a storage pillar, the H_C is tunable by a negative electric potential, and ranged from a storage area of high H_C to a writing area of relatively small H_C within an available head field range. In additional, the patterned pillars are isolated in write or read process because of the parallel potential channel design. The parallel potential channel is designed to switch the write and read process by changing the supplied electric potential for each pillar that can avoid the exchange coupling between pillars. In these design, the potential controllable magnetic pillars can be structured as three-dimensional stacking like many electronic devices[34] which improve the amount of pack clusters and enhance the areal density in a disc. Combining the solution process and controlling the electric potential for the operation of a magnetic device is a viable technique for achieving a highly controlled efficiency and a lower power consumption with a reduced cost of production. The developed EPTMR shows promise for use in applications in which the solution process is combined with electric potential control for magnetic data storage.

After waiting for a certain time at a suitable potential for Co deposition, a linear potential scan in the positive potential direction is performed to strip off the Co from the film. Anodic peaks from cyclic voltammograms (CV) for strip off measurements for Co/Pt(111) thinner than 18 nm are shown in Fig. 2a. The thickness of the cobalt
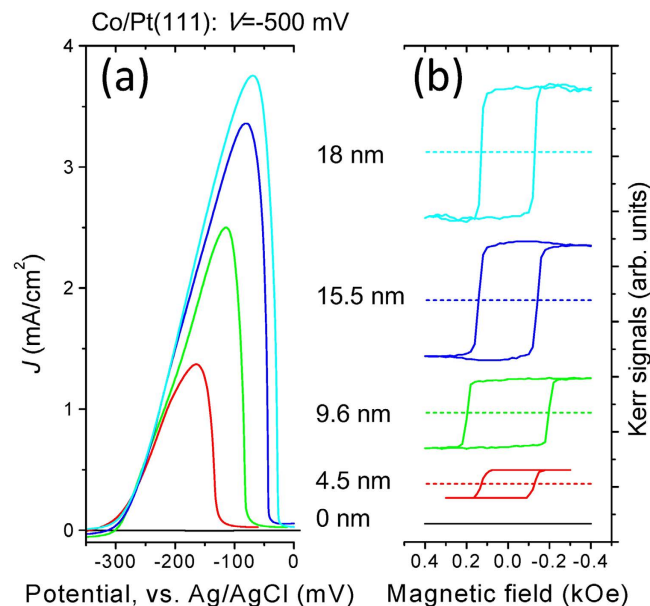
Figure 2. (**a**) The CV of strip off measurements for Co/Pt(111). (**b**) Kerr signals versus the magnetic field measured at $V = -500\,mV$ for Co/Pt(111) in both the longitudinal (solid lines) and polar (dashed lines) configurations.

can be obtained from the strip off method by measuring the quantity of electric charge, by integrating the charge under the anodic peak[28,35]. Figure 2b shows Kerr signals versus the magnetic field measured at electric potential $V = -500\,mV$ for a Co/Pt(111) layer thinner than 18 nm. No hysteresis is detected in the polar configuration. Hysteresis occurs only in the longitudinal configuration. This shows that the easy axis of magnetization lies on the surface plane. Shape anisotropy is dominant for the Co/Pt(111) in this thickness range[36,37].

Figure 3a shows the saturated Kerr intensities in both the longitudinal and polar configurations versus the Co thickness (t_{Co}). As the t_{Co} increases, the saturated Kerr intensity in the longitudinal configuration increases between 4.5 and 18 nm, due to the relation between the magnetization and the thickness of the ferromagnetic layers[38]. This phenomenon has also been reported for Co/Cu(001) films in electrolytic conditions[39] and for Mn-doped ZnO films[40]. The relation between the saturation magnetization (M_S) and t_{FM} can be expressed by

$$M_S \propto t_{FM} \tag{1}$$

by considering the amount of magnetic moments in a ferromagnetic layer[38–42]. A plot of the coercive force of Co/Pt(111) versus t_{Co} is shown in Fig. 3b. The value for H_C increases rapidly with increasing t_{Co} below 6.8 nm. From the literature, Bloch wall energy density decreases with increasing film thickness because of the increased magnetostatic energy due to the appearance of charged surface above and below the wall, while the Néel wall energy shows opposite trend because of the proportional relation with the area of the charged surface inside the film[43]. The analysis of the demagnetization energy for Néel-wall regime shows that the increase of the H_C by increasing the film thickness[44,45]. As the thicknesses of magnetic layers increase, the change from of domain-wall types from Néel wall to Bloch wall has been reported for different magnetic materials in nanometer thicknesses[43–47]. For Co/Pt(111) films thicker than 6.8 nm, H_C decreases monotonously which follows Bloch wall behavior[35,44,48]. By increasing t_{FM}, the increase in H_C to a maximum at around several nanometers followed by a monotonous decrease for thicker films has been previously reported and can be described by changing the domain wall type from a Néel wall to a Bloch wall[43].

In order to elucidate the role of the electric potential on the magnetic properties of Co/Pt(111) in Néel-wall and in Bloch-wall regimes, Fig. 4a and b show Kerr signals versus the magnetic field for 4.5 and 6.8 nm Co/Pt(111), respectively. For Co/Pt(111) in the Néel-wall regime ($t_{Co} = 4.5\,nm$), no significant change in H_C is detected at different electric potentials. The Néel-wall is related to the film thickness in order to minimize the magnetostatic energy. At a sufficiently small film thickness, the magnetostatic energy is no longer significant and the Néel-wall is stabilized. In addition, the energy density of the Néel-wall is related to its magnetization and film thickness[43]. Therefore, the electric potential might not easily induce a change in the Néel-wall in few hundred millivolts. For Co/Pt(111) in the Bloch-wall regime ($t_{Co} = 6.8\,nm$), an electric potential induced change in H_C occurs. For a larger negative electric potential ($V = -500\,mV$), the value for H_C is smaller. This result provides strong evidence for the negative electric potential induced depression in H_C for Co/Pt(111) in the Bloch-wall regime. Variations in H_C are shown in Fig. 4c for Co/Pt(111) in the Bloch-wall regime under conditions where the electric potential is repeatedly changed between $V = -500$ and $-400\,mV$. The jump in H_C between 0.42 and 0.48 kOe is highly reproducible within hours of the start of the experimental tests. At this electric potential range, the typical current is around few $\mu A/cm^2$. The heating power density by the electric current is less than a few $\mu W/cm^2$ and therefore the effects of thermal annealing can be neglected. In additional, in the Bloch-wall regime, the films

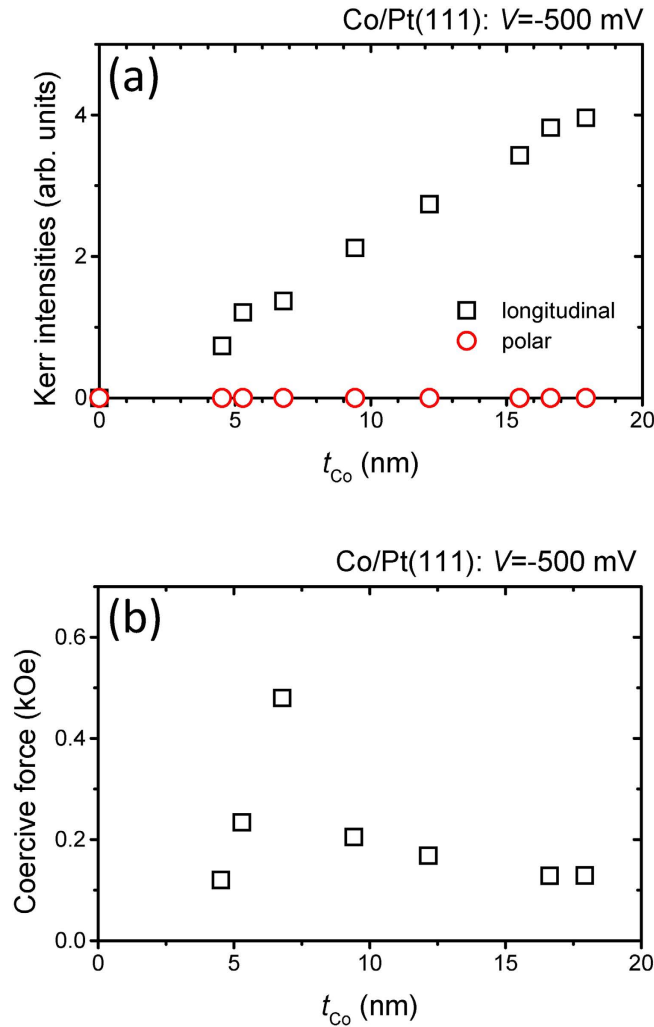**Figure 3.** (**a**) Saturated Kerr intensities versus the thickness of the Co layer in both the longitudinal and polar configurations. (**b**) Coercive force versus Co thickness in the longitudinal configuration.

are robust against variations in the electric potential for magnetic switching[44]. We therefore conclude that controlling H_C by means of the electric potential for magnetic films in the Bloch-wall regime represents a possible route for preparing spintronic switching devices. In the following discussions for the electric potential induced phenomena, we focus on Co/Pt(111) in the Bloch-wall regime.

As shown in Fig. 5a for Co/Pt(111) with t_{Co} between 7 and 18 nm, the H_C measured at both $V = -500$ and -400 mV decrease monotonously with increasing t_{Co}. At $V = -500$ mV for an individual t_{Co}, the reduction in H_C is more pronounced. By tuning the electric potential V, the electric field E applied to the specimen can be adjusted. The change in the coercive force (ΔH_C) at electric fields E_1 and E_2 can be defined as

$$\Delta H_C \equiv H_C(E_2) - H_C(E_1). \tag{2}$$

Figure 5b shows plots of ΔH_C versus t_{Co} where the electric fields E_1 and E_2 correspond to the electric potentials $V_1 = -500$ mV and $V_2 = -400$ mV, respectively. The value for ΔH_C decreases with increasing t_{Co}. In a further analysis of the data in Fig. 5b by taking the logarithms of both the ΔH_C and t_{Co}, a well linear relation between $\ln(\Delta H_C)$ and $\ln(t_{Co})$ is observed, as shown in Fig. 5c. A slope of -2.00 ± 0.06 was obtained from the linear fitting of the data. This shows that the ΔH_C is proportional to the inverse of the square of t_{Co}. Based on the above experimental evidence, we proposed an EPT-MAE model to explain the inverse square relation between the electric potential tuned H_C and the thickness of the ferromagnetic layer. Detailed discussions are below.

Both the magnetic anisotropy and the imperfections in ferromagnetic materials give rise to hysteresis loss and an increase in the coercive force[44]. Being an upper limit of the H_C, an easy-axis magnetization process results in a square M-H loop, and is characterized in the single domain behavior or pinned wall limit by rotational hysteresis, i.e.,

$$(H_C)_{max} = 2K_u/M_S \tag{3}$$

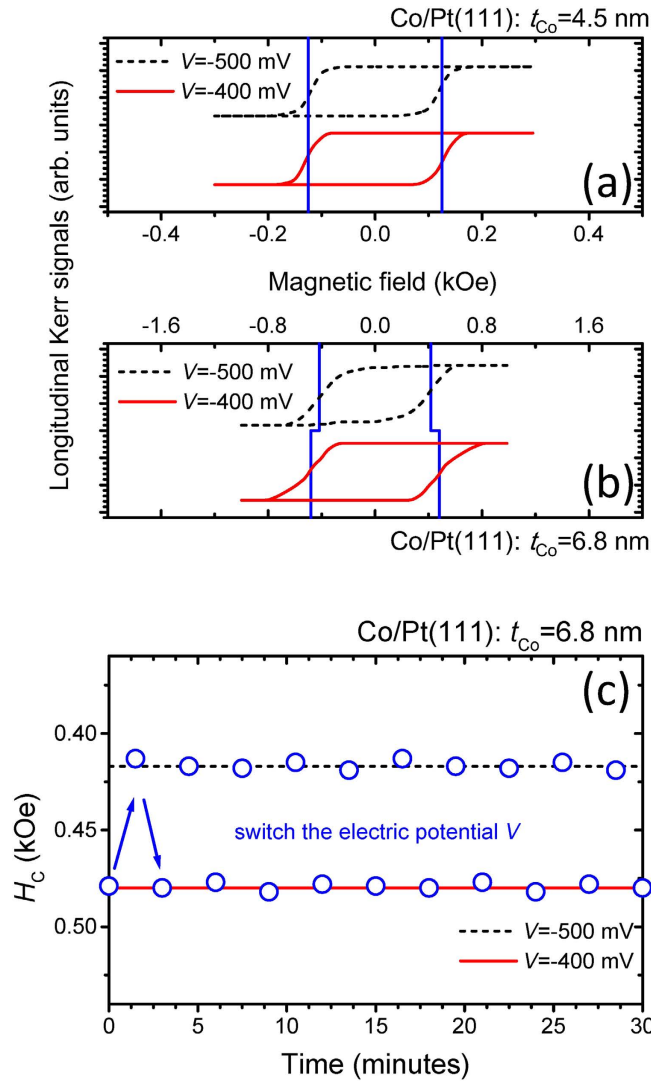**Figure 4.** Kerr signals versus the magnetic field measured at $V = -500$ and $-400\,\text{mV}$ for (**a**) 4.5 and (**b**) 6.8 nm Co/Pt(111) in the longitudinal configuration. (**c**) Variations of the H_C for 6.8 nm Co/Pt(111) under conditions of continuously changing electric potential $V = -500$ and $-400\,\text{mV}$.

where K_u is the MAE of the ferromagnetic layer[43]. By considering the hysteresis loss energy for the pinning of the domain wall motion, the lower limit of the coercive force can be expressed by

$$(H_C)_{\min} = n\varepsilon/2M_S \tag{4}$$

where n is the amount of pinning sites and ε is the pinning energy for a domain wall motion[44]. Combining Eqs (3) and (4), the coercive force can be expressed as

$$H_C = p\,[2K_u/M_S] + (1 - p)\,[n\varepsilon/2M_S] \tag{5}$$

where p ($0 \leq p \leq 1$) is the percentage of the contribution of the magnetic anisotropy energy. By tuning the electric potential applied to a ferromagnetic film, previous investigations indicate that the corresponding magnetoresistance[49,50], Hall effects[51,52] and magnetization switching[10,23,28] are highly reproducible. By choosing suitable electric potential ranges, the changing of pinning sites such as impurities, grain boundary, dislocations, and voids in the ferromagnetic films can be avoided[10,23,28,49–52]. Assuming that pinning sites are independent of the applied electric potential, the pinning of domain wall motion related to hysteresis loss energy can be neglected for an analysis of ΔH_C. Therefore, from Eq. (5), ΔH_C can be expressed by

$$\Delta H_C \propto \Delta K_u/M_S. \tag{6}$$

Because the M_S is proportional to t_{FM} as shown in Eq. (1), the relation between the t_{FM} and the ΔH_C can be expressed by
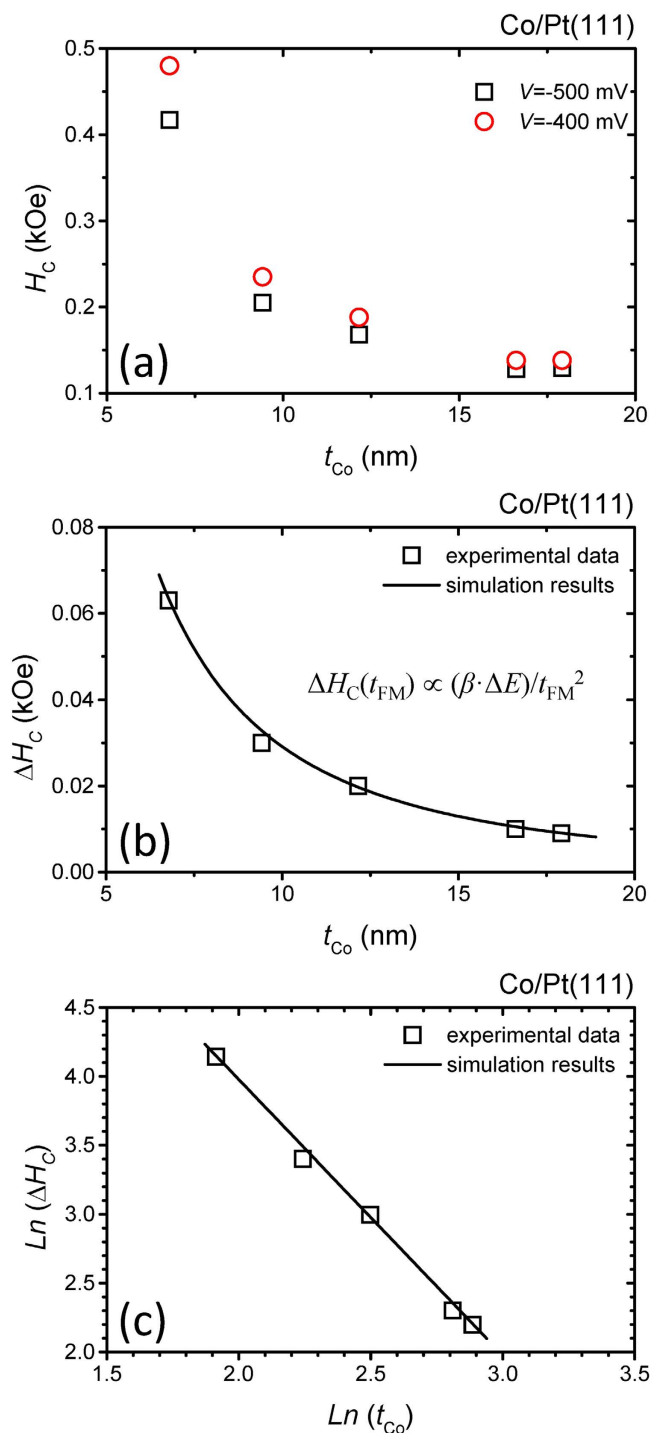
Figure 5. (**a**) H_C versus Co thickness for Co/Pt(111) with Co thickness thicker than 6.8 nm measured at $V = -500$ and -400 mV in the longitudinal configuration. (**b**) The experimental data and simulation results for ΔH_C versus the thickness of the Co layer. (**c**) The experimental data and simulation results for the $\ln(\Delta H_C)$ versus $\ln(t_{Co})$.

$$\Delta H_C \propto \Delta K_u / t_{FM} \qquad (7)$$

In previous reports, the first principle calculations for Fe and Co films on Pt(111) show that the MAE is enhanced when the electric field E is increased[30]. The electric voltage effect on MAE of magnetic layers is expected via charge redistribution among different electron d-orbitals (some or all of d_{xy}, d_{yz}, d_{xz}, d_{z^2}, and $d_{x^2-y^2}$) in the presence of electric field[53]. For ultrathin films, it has been reported that the absorption atoms such as H^+, OH^- and CO on the top of Co can influence the interface MAE via controllable electric field effect[54,55]. In this report, we
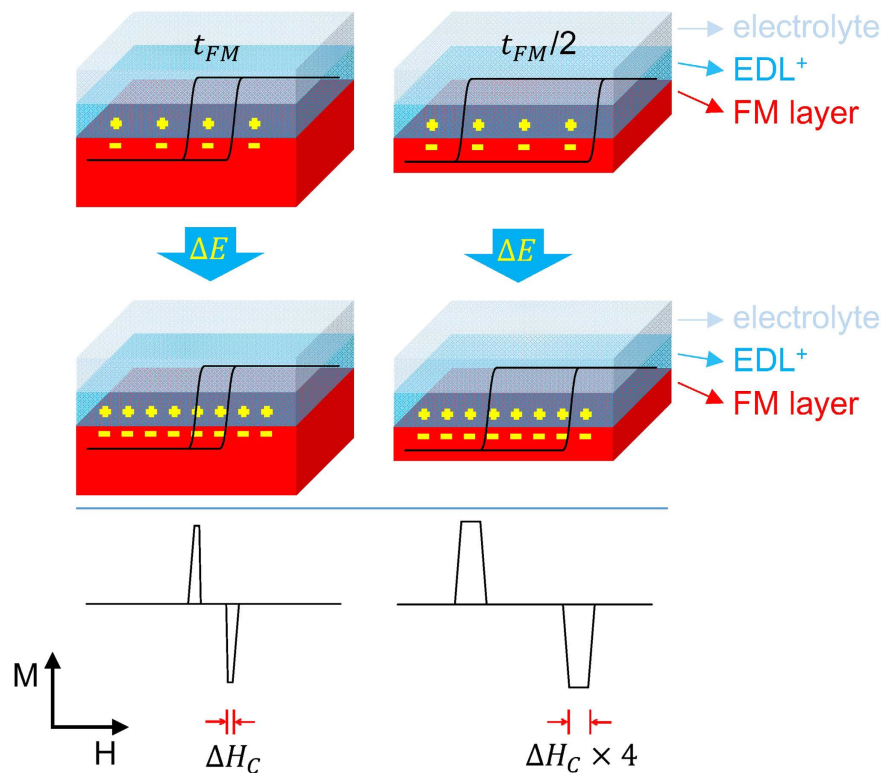
Figure 6. A schematic plot shows the electric potential induced change of the coercive force for ferromagnetic layers with different thicknesses in the Bloch-wall regime.

start from Co/Pt(111) thicker than 4.5 nm where the MAE contains both the bulk and interfacial contributions. The adsorbed species are H^+ and K^+ in the electrolyte while the large electric field created by the electrical double layer near the electrode surface is responsible to the change of the MAE of the magnetic system. The electric field applied on the specimen can be adjusted by tuning the electric potential V. The change in the electric field (ΔE) can be defined as

$$\Delta E \equiv E_2 - E_1. \tag{8}$$

Under different electric fields, the MAEs are different. In this study, the magneto-optical Kerr effect (MOKE) measurements were carried out at electric potentials $V_1 = -500\,\text{mV}$ and $V_2 = -400\,\text{mV}$. By further considering the thickness of the ferromagnetic layer, the relation between the change in magnetic anisotropy energy ΔK_u at the electric fields E_1 and E_2 (corresponding to $V_1 = -500\,\text{mV}$ and $V_2 = -400\,\text{mV}$, respectively) and the change in the electric field ΔE can be expressed as

$$\Delta K_u \propto (\beta \cdot \Delta E)/t_{FM} \tag{9}$$

where β is the interfacial magnetic anisotropy energy coefficient[31]. By substituting Eq. (9) into Eq. (7), the dependence of ΔH_C on layer thickness can be expressed as

$$\Delta H_C \propto (\beta \cdot \Delta E)/t_{FM}^2. \tag{10}$$

From the discussions of the electric field induced change of MAE, the ΔH_C versus t_{FM} shows an inverse square relation, as shown in Eq. (10). This relation is in good agreement with the experimental data in Fig. 5c where the slope of a plot of $\ln(\Delta H_C)$ versus $\ln(t_{Co})$ is $-2.00 + 0.06$. This result shows that combining MAE and electric field effects can successfully explain the inverse square relation between the ΔH_C and the t_{FM}.

Based on Eqs (7, 9, and 10), an EPT-MAE model that explains the relation between the electric potential tuned H_C and t_{FM} is proposed and is schematically illustrated in Fig. 6. For a smaller t_{FM}, the electric potential induced change in H_C is larger, as indicated in Eq. (7). The electric potential induced change of MAE again magnifies the change in H_C as suggested in Eq. (9). The resultant effects are responsible for the inverse square relation between ΔH_C and t_{FM} in Eq. (10). In the left panel of Fig. 6, a more negative electric potential shows the effect of reduction of H_C. Compared to the right panel of Fig. 6 for a half t_{FM}, the electric potential induced ΔH_C is enhanced by four times. This shows that the electric potential induced ΔH_C is much more pronounced for thinner ferromagnetic layers. From a technological point of view, by changing the electric potential in ferromagnetic layers with smaller thicknesses, a higher controlling efficiency of the tunable H_C is demonstrated in our apparatus. The establishment

of the EPT-MAE model provides insights into our knowledge of the relation between electric potential tuning H_C, the ferromagnetic layer thickness, and associated mechanisms.

For magnetic recording applications, superparamagnetic behavior is the limitation for further reducing the volume of a magnetic bit, but EPTMR is a possibility, as shown in Fig. 1. From the literature, in order for magnetic grains in a typical size distribution to remain stable for ~10 years, the ambient temperature stability factor $K_u V/k_B T$ needs to be larger than 70 for a commercial device[9]; where V is the volume of a nanoparticle; k_B is the Boltzmann constant; and T is the sample temperature. To enhance the areal density of a magnetic recording disc, increasing the MAE is the key point. When using a material with a higher MAE, a higher writing field is necessary, but this is a disadvantage for real applications. By employing an electric potential tuned mechanism, the findings reported here show that 100 mV can reduce the coercive force by 15% for thin magnetic films (6.8 nm Co/Pt(111) as an example) in the Bloch wall regime. In practice, by using EPTMR, it is possible to create stable recording media with a high writing ability.

In conclusion, for Co/Pt(111) of nanometer thickness in the Bloch-wall regime, a depression in H_C is detected when a negative electric potential is applied in an electrolytic condition. For Co/Pt(111) under conditions of a continuously changing electric potential, the increase in H_C between two states is highly reproducible. As the value for t_{FM} increases, both the H_C measured at $V = -500$ and -400 mV decrease monotonously. The reduction of H_C for an individual t_{Co} is more pronounced at a more negative potential. An electric potential tuned H_C and t_{FM} have an inverse square relationship with one another. By changing the electric potential in ferromagnetic layers with smaller thicknesses, a higher controlling efficiency of tunable H_C is achieved. Assuming that the pinning domains are independent of the applied electric potential, an EPT-MAE model in which the MAE and the electric field effects are combined is established. This provides insights into our knowledge of the relation between electric potential tuning H_C and the thickness of the ferromagnetic layer. The implementing of EPTMR is a potentially promising route for applications combining a solution process and electric potential control in magnetic data storage.

Methods

A platinum crystal was oriented within 0.5° of the [111] direction as checked by x-ray diffraction. The diameter of the crystal is 8 mm while the thickness is 2 mm. This specimen size is suitable for the designed apparatus for the MOKE measurements in electrochemical environments[28,35,56]. Before loading into the electrochemical cell, the surface of the crystal was mechanically polished with alumina powder with a diameter down to 0.05 μm and was then annealed using a hydrogen torch. The details of the process for preparing Pt electrode can be found in the literature[28,57–59]. All solutions were prepared with high purity chemicals (HCl and $CoCl_2$) and ultra-pure water (>18 MΩ cm). To avoid contamination by oxygen, the solutions were purged with high purity argon for 1 hr before the experiments. The electrochemical cell used for the CV and MOKE measurements was developed and built in our laboratory[34,56]. Pt and Ag wires were used as the counter electrode and the reference electrode, respectively. The electricity of the standard three-electrode setup was controlled by a potentiostat that was constructed in Bonn[34,56,60,61]. The CV of the Pt(111) electrode in a pure supporting electrolyte containing HCl and KCl, and with a $CoCl_2$ additive are shown in the Supplementary Information 1. For the condition of the film deposition, by comparing the CV for specimens in electrolytes with and without $CoCl_2$, the electric potential range that is suitable for the electrodeposition of Co/Pt(111) was determined. The Co layer was electrodeposited at an electric potential more negative than -700 mV for a pre-determined time, depending on the thickness of the layer. The potential range for MOKE measurements was chosen to be between -400 and -600 mV to avoid the possible deposition/dissolution of the Co deposits. A He–Ne laser with a wavelength of 632.8 nm was used as the light source for the MOKE measurements. The Kerr signals as a function of magnetic field were measured by a photodiode and recorded by a computer-controlled multimeter to generate the hysteresis loops.

By applying an electric potential, an electrical double layer (EDL) near the electrode surface was established[62]. The thickness of the EDL was in the nanometer scale, thus permitting hundreds of millivolts to create an electric field as large as 10^8 V/m[25,63]. A schematic plot in Supplementary Information 2 elucidates the specimen structure where the electric field influences the ferromagnetic layer supported on the Pt electrode through the establishment of the EDL. The electric field is responsible for the change in MAE and the related change in the H_C. Surface species are different in different electrolytes, and the effects of point of a zero charge (PZC) need to be taken into consideration. In this report, we used the same electrolyte and the same electrochemical conditions, the PZC was not altered. Discussions of the EDL as well as the PZC can be found in the Supplementary Information 2 and may be of importance for further applications in the case for solution processes.

References

1. Scheunert, G. *et al.* A review of high magnetic moment thin films for microscale and nanotechnology applications. *Appl. Phys. Rev.* **3,** 011301 (2016).
2. Coughlin, T. HDD Annual Unit Shipments Increase In 2014, (Forbes online 2015), http://www.forbes.com/sites/tomcoughlin/2015/01/29/hdd-annual-unit-shipments-increase-in-2014/ (Date of access: 20/05/2016).
3. Shiroishi Y. *et al.* Future Options for HDD Storage. *IEEE Trans. Magn.* **45,** 3816 (2009).
4. Auerbach1, E., Gider, S., Albuquerque, G. & Mauri, D. Influence of Parasitic Capacitance on Single and Dual 2-D Magnetic Recording Read Head Performance. *IEEE Trans. Magn.* **52,** 3000804 (2016).
5. Wang, Y., Victora, R. H. & Faith Erden, M. Two-Dimensional Magnetic Recording With a Novel Write Precompensation Scheme for 2-D Nonlinear Transition Shift. *IEEE Trans. Magn.* **51,** 3000507 (2015).
6. Shi, J., Liu, B., Li, P., Ng, L. Y. & Shen, S. Near-Field Energy Extraction with Hyperbolic Metamaterials. *Nano Lett.* **15,** 1217 (2015).
7. Dwivedi, N. *et al.* Understanding the Role of Nitrogen in Plasma-Assisted Surface Modification of Magnetic Recording Media with and without Ultrathin Carbon Overcoats. *Sci. Rep.* **5,** 7772 (2015).
8. Challener, W. A. *et al. Nat. Photonics* **3,** 220 (2009).
9. Kryder, M. H. *et al.* Heat Assisted Magnetic Recording. *Proc. IEEE* **96,** 1810 (2008).

10. Okamoto, S., Kikuchi, N., Furuta, M., Kitakami, O. & Shimatsu, T. Microwave assisted magnetic recording technologies and related physics. *J. Phys. D: Appl. Phys.* **48,** 353001 (2015).
11. Zhu, J. G., Zhu, X. & Tang, Y. Microwave assisted magnetic recording. *IEEE Trans. Magn.* **44,** 125 (2008).
12. Velez, C., Torres-Díaz, I., Maldonado-Camargo, L., Rinaldi, C. & Arnold, D. P. Magnetic Assembly and Cross-Linking of Nanoparticles for Releasable Magnetic Microstructures. *ACS nano* **9,** 10165 (2015).
13. Xue, X., Wang, J. & Furlani, E. P. Self-Assembly of Crystalline Structures of Magnetic Core−Shell Nanoparticles for Fabrication of Nanostructured Materials. *ACS Appl. Mater. Interfaces* 7, 22515 (2015).
14. Henderson, J., Shi, S., Cakmaktepe, S. & Crawford, T. M. Pattern Transfer Nanomanufacturing Using Magnetic Recording for Programmed Nanoparticle Assembly. *Nanotechnology* **23,** 185304 (2012).
15. Albrecht, T. R. *et al.* Bit-Patterned Magnetic Recording: Theory, Media Fabrication, and Recording Performance. *IEEE Trans. Magn.* **51,** 0800342 (2015).
16. Liu, T. M. *et al.* Nanoscale Confinement of All-Optical Magnetic Switching in TbFeCo - Competition with Nanoscale Heterogeneity. *Nano Lett.* **15,** 6862 (2015).
17. Lin, W. S. *et al.* Photomagnetic Carbon Nanotubes at Ambient Conditions. *J. Phys. Chem. C* **119,** 20673 (2015).
18. Ohkoshi, S., Imoto, K., Tsunobuchi, Y., Takano, S. & Tokoro, H. Light-induced spin-crossover magnet. *Nature Chem.* **3,** 564 (2011).
19. Cormier, M. *et al.* Electric-field-induced magnetization reorientation in a (Ga,Mn)As/(Ga,Mn)(As,P) bilayer with out-of-plane anisotropy. *Phys. Rev. B* **90,** 174418 (2014).
20. Gerhard, L., Bonell, F., Wulfhekel, W. & Suzuki, Y. Influence of an electric field on the spin-reorientation transition in Ni/Cu(100). *Appl. Phys. Lett.* **105,** 152903 (2014).
21. Meng, H., Naik, V. B., Liu, R. & Han, G. Electric field control of spin re-orientation in perpendicular magnetic tunnel junction-CoFeB and MgO thickness dependence. *Appl. Phys. Lett.* **105,** 042410 (2014).
22. Bauer, U. *et al.* Magneto-ionic control of interfacial magnetism. *Nature Mater.* **14,** 174 (2015).
23. Chiba, D., Yamanouchi, M., Matsukura, F. & Ohno, H. Electrical Manipulation of Magnetization Reversal in a Ferromagnetic Semiconductor. *Science* **301,** 943 (2003).
24. Chiba, D. & Ono, T. Control of magnetism in Co by an electric field. *J. Phys. D: Appl. Phys.* **46,** 213001 (2013).
25. Obinata, A. *et al.* Electric-field control of magnetic moment in Pd. *Sci. Rep.* **5,** 14303 (2015).
26. Weisheit, M. *et al.* Electric Field–Induced Modification of Magnetism in Thin-Film Ferromagnets. *Science* **315,** 349 (2007).
27. Shimamura, K. *et al.* Electrical control of Curie temperature in cobalt using an ionic liquid film. *Appl. Phys. Lett.* **100,** 122402 (2012).
28. Chang, C. H. T., Kuo, W. H. & Tsay, J. S. Electric field modifications on the coercive force for electrochemical etched Co/Pt(111) films, Surf. *Coating Technol.* **303,** 136 (2016).
29. Matsukura, F., Tokura, Y. & Ohno, H. Control of magnetism by electric fields. *Nature Nanotech.* **10,** 209 (2015).
30. Suzuki, S., Shiota, M., Fukuchi, Y. & Seki, S. First-Principles Study of Electric Field Effects on Magnetic Anisotropy in Ultrathin Ferromagnetic TM (TM = Fe, Co) Films on Pt(111) Underlayer. *J. Phys. Soc. Jpn.* **84,** 014709 (2015).
31. Bai, Z. *et al.* Magnetocrystalline anisotropy and its electric-field assisted switching of Heusler-compound-based perpendicular magnetic tunnel junctions. *New J. Phys.* **16,** 103033 (2014).
32. Yoshikawa, D., Obata, M., Taguchi, Y., Haraguchi, S. & Oda, T. Possible origin of nonlinear magnetic anisotropy variation in electric field effect in a double interface system. *Appl. Phys. Express* **7,** 113005 (2014).
33. Maruyama, T. *et al.* Large voltage-induced magnetic anisotropy change in a few atomic layers of iron. *Nature Nanotech.* **4,** 158 (2009).
34. Kim, J. *et al.* A stacked memory device on logic 3D technology for ultra-high-density data storage. *Nanotechnology* **22,** 254006 (2011).
35. Mangen, T., Bai, H. S. & Tsay, J. S. Structures and magnetic properties for electrodeposited Co ultrathin films on copper. *J. Magn. Magn. Mater.* **322,** 1863 (2010).
36. Yamamoto, N., Manohara, H. & Platzman, E. Magnetically anisotropic additive for scalable manufacturing of polymer nanocomposite: iron coated carbon nanotubes. *Mater. Res. Express* **3,** 025004 (2016).
37. Johnson, M. T., Bloemen, P. J. H., den Broeder, F. J. A. & de Vries, J. J. Magnetic anisotropy in metallic multilayers. *Rep. Prog. Phys.* **59,** 1409 (1996).
38. Qiu, Z. Q. & Bader, S. D. Surface magneto-optic Kerr effect. *Rev. Sci. Instrum.* **71,** 1243 (2000).
39. Schindler, W. & Kirschner, J. Ultrathin magnetic films: Electrochemistry versus molecular-beam epitaxy. *Phys. Rev. B* **55,** R1989 (1997).
40. Straumal, B. B. *et al.* Magnetization study of nanograined pure and Mn-doped ZnO films: Formation of a ferromagnetic grain-boundary foam. *Phys. Rev. B* **79,** 205206 (2009).
41. Almasi-Kashi, M., Ramazani, A., Kheyri, F. & Jafari-Khamse, E. The effect of magnetic layer thickness on magnetic properties of Fe/Cu multilayer nanowires. *Mater. Chem. Phys.* **144,** 230 (2014).
42. Liu, C., Moog, E. R. & Bader, S. D. Polar Kerr-Effect Observation of perpendicular Surface Anisotropy for Ultrathin fcc Fe Grown on Cu(100). *Phys. Rev. Lett.* **60,** 2422 (1988).
43. O'Handley, R. C. *Modern Magnetic Materials: Principles and Applications* (Wiley: New York 1999).
44. Jiles, D. *Introduction to Magnetism and Magnetic Materials* (3rd ed., CRC Press 2016).
45. Zhao, Y. P., Gamache, R. M., Wang, G. C., Lu, T. M., Palasantzas, G. & Hosson, J. & Th, M. De. Effect of surface roughness on magnetic domain wall thickness, domain size, and coercivity. *J. Appl. Phys.* **89,** 1325 (2001).
46. Castano, F. J., Stobiecki, T., Gibbs, M. R. J., Czapkiewicz, M., Wrona, J. & Kopcewicz, M. Magnetic and morphological properties of ultrathin Fe layers in Zr/Fe/Zr trilayer structures. *Thin Solid Films* **348,** 233 (1999).
47. Romera, M., Ranchal, R., Ciudad, D., Maicas, M. & Aroca, C. Magnetic properties of sputtered Permalloy/molybdenum multilayers. *J. Appl. Phys.* **110,** 083910 (2011).
48. Niño, M. Á. *et al.* Surfactant-assisted epitaxial growth and magnetism of Fe films on Cu(111). *J. Phys.: Condens. Matter* **20,** 265008 (2008).
49. Tsuchiya, T. *et al. In Situ* Tuning of Magnetization and Magnetoresistance in Fe_3O_4 Thin Film Achieved with All-Solid-State Redox Device. *ACS Nano* **10,** 1655 (2016).
50. Zhou, W. *et al.* Multilevel Resistance Switching Memory in $La_{2/3}Ba_{1/3}MnO_3/0.7Pb(Mg_{1/3}Nb_{2/3})O$-$0.3PbTiO_3(011)$ Heterostructure by Combined Straintronics-Spintronics. *ACS Appl. Mater. Interfaces* **8,** 5424 (2016).
51. Chen, C. H., Lin, C. H., Yang, Y. S. & Hwang, C. H. Manipulating Polycrystalline Silicon Nanowire FET Characteristics by Light Illumination. *J. Phys. Chem. C* **120,** 5783 (2016).
52. Tang, J. *et al.* Versatile Fabrication of Self-Aligned Nanoscale Hall Devices Using Nanowire Masks. *Nano Lett.* **16,** 3109 (2016).
53. Wang, D. S., Wu, R. & Freeman, A. J. First-principles theory of surface magnetocrystalline anisotropy and the diatomic-pair model. *Phys. Rev. B* **47,** 14932 (1993).
54. Di, N., Kubal, J., Zeng, Z., Greeley, J., Maroun, F. & Allongue, P. Influence of controlled surface oxidation on the magnetic anisotropy of Co ultrathin films. *Appl. Phys. Lett.* **106,** 122405 (2015).
55. Tournerie, N., Engelhardt, A., Maroun, F. & Allongue, P. Probing the electrochemical interface with *in situ* magnetic characterizations: A case study of Co/Au(111) layers. *Surf. Sci.* **631,** 88 (2015).
56. Lin, C. L., Wu, A. W., Wang, Y. C., Tseng, Y. C. & Tsay, J. S. Spin reorientation transitions and structures of electrodeposited Ni/Cu(100) ultrathin films with and without Pb additives. *Phys. Chem. Chem. Phys.* **15,** 2360 (2013).

57. Clavilier, J., Armand, D., Sun, S. G. & Petit, M. Electrochemical adsorption behaviour of platinum stepped surfaces in sulphuric acid solutions. *J. Electroanal. Chem.* **205,** 267 (1986).
58. Tanaka, S., Yau, S. L. & Itaya, K. *In-situ* scanning tunneling microscopy of bromine adlayers on Pt(111). *J. Electroanal. Chem.* **396,** 125 (1995).
59. Yen, P. Y. *et al.* Epitaxial Electrodeposition of Cobalt on a Pt(111) Electrode Covered with a Cu(111) Film. *J. Phys. Chem. C* **15,** 23802 (2011).
60. Tsay, S. L. *et al.* Molecular structures of dicarboxylated viologens on a Cu(100) surface during an ongoing charge transfer reaction. *Phys. Chem. Chem. Phys.* **12,** 14950 (2010).
61. Pham, D. T. *et al.* Quasi-Reversible Chloride Adsorption/Desorption through a Polycationic Organic Film on Cu(100). *J. Phys. Chem. C* **111,** 16428 (2007).
62. Bard, A. J. & Faulkner, L. R. *ELECTROCHEMICAL METHODS: Fundamentals and Applications*, (Wiley: New York 2001).
63. Jackson, J. D. *Classical Electrodynamics*, (3rd ed., John Wiley and Sons: New York 1999).

Acknowledgements

Author Contributions

C.H.T.C. and W.H.K. set up the measurement apparatus. C.H.T.C., W.H.K., and Y.C.C. carried out the experiments. J.S.T. planed and supervised the study. C.H.T.C. and J.S.T. wrote the manuscript with reviewing by S.L.Y. All authors participated in discussing the results and commented on the manuscript.

Additional Information

Supplementary information accompanies this paper at http://www.nature.com/srep

Competing Interests: The authors declare no competing financial interests.

How to cite this article: Chang, C.-H.-T. *et al.* Tuning coercive force by adjusting electric potential in solution processed Co/Pt(111) and the mechanism involved. *Sci. Rep.* **7**, 43700; doi: 10.1038/srep43700 (2017).

Publisher's note: Springer Nature remains neutral with regard to jurisdictional claims in published maps and institutional affiliations.